ZANCO Journal of Pure and Applied Sciences

TYPE Original article
DOI http://dx.doi.org/10.21271/ZJPAS.37.4.4

OPEN ACCESS

*Corresponding author

Abbas Hussein Rostam

abbas.rostam@su.edu.krd

RECEIVED :10 /02 /2025
ACCEPTED :12/05/ 2025
PUBLISHED :31/ 08/ 2025

KEYWORDS:

Green Synthesis, CuO NPs, Curcuma Longa, Nanoparticles Green Synthesis.

Green Synthesis and Characterization of CuO Nanostructures Using *Curcuma longa* Extract: Optimization of Precursor Concentration

Abbas Hussein Rostam

Department of General Science, Collage of Basic Education, Salahaddin University-Erbil, Kurdistan Region, Iraq

ABSTRACT

CuO nanoparticles were synthesized via a green route using Curcuma longa extract as both reducing and capping agents. The influence of precursor concentration (0.025–0.1 M) on the morphology, size distribution, and structural quality of the nanostructures was systematically investigated. Characterization by SEM, XRD, FTIR, UV–Vis spectroscopy, and EDX identified an optimal sheet-like morphology at 0.05 M (sample S2), with an average thickness of 18 nm, minimal aggregation, and high homogeneity. FTIR spectra confirmed characteristic Cu–O stretching vibrations, and XRD patterns revealed a phase-pure monoclinic CuO crystal structure. UV–Vis analysis showed a distinct absorption peak at 376 nm corresponding to the optical band gap, while EDX confirmed elemental purity. These results demonstrate that Curcuma longa–mediated synthesis offers an eco-friendly, scalable approach for producing CuO nanostructures suitable for catalysis, sensing, and environmental remediation applications.

.

1.Introduction

Copper oxide nanoparticles (CuO NPs) are a key group of nanomaterials that are characterized by a large surface to volume ratio, great catalytic activity, antimicrobial activity, and good electrical conductivity (Gota, 2024, S Naz, 2023). These distinctive properties of CuO NPs make them promising materials for specific applications such as environmental remediation, catalysis, energy storage devices, sensors, and biomedical applications. CuO NPs are also extensively investigated for pollutant degradation and for potential applications in cancer therapy and drug delivery (Bhuvaneshwari, 2018, Grigore, 2016).

The semiconductor properties of CuO NPs with a narrow bandgap of about 1.2 eV enable them to engage in redox reactions and be useful for catalytic and sensing applications (Fuku, 2018). CuO NPs also exhibit improved magnetic and electronic properties that can be useful for applications in high-performance batteries, supercapacitors, and magnetic storage units. In addition, thermal conductivity and thermal stability make them excellent materials for thermal management systems applications (Jayasimha, 2024, Mishra, 2022).

The synthesis of CuO NPs is a crucial step that directly influences their properties and efficacy in various applications. Conventional methods for synthesizing CuO NPs generally involve chemical methods like precipitation, sol-gel, and hydrothermal methods that usually involve toxic reagents and energy-consuming processes (ZHIAN, 2024, Okoye, 2023, Mathanmohun, 2024). These methods form nanoparticles with desired properties but are also connected with severe environmental and health risks. There has been a transition to sustainable, low-cost, and environmentally friendly green synthesis techniques. Green synthesis techniques utilize biological sources like plant extracts, microbes, and biomolecules as reducing and stabilizers for nanoparticle formation. Such methods are environmentally friendly and promote nanoparticle formation with enhanced biocompatibility and decreased toxicity (Jeevanandam, 2022).

Various studies have confirmed the efficacy of green synthesis methods to generate quality CuO NPs. (Shukla, 2022) prepared CuO NPs using Azadirachta indica (neem) extract that exhibited excellent antimicrobial activity. Alhamdi et al. demonstrated that Moringa oleifera extract can be employed to synthesize CuO NPs with improved photocatalytic activity for environmental remediation (Alhamdi et al., 2024). The studies establish the capability of plant extracts to control nanoparticle properties for particular applications. Progress in recent times has been on optimizing synthesis conditions like time, temperature, and precursor concentration to enhance control of particle size, shape, and distribution.

Curcuma longa or turmeric has been of particular interest to plant-based processes because it is rich in bioactive compounds such as polyphenols, flavonoids, and curcuminoids (Jayarambabu, 2020). They serve a dual function by reducing metal ions to nanoparticle size and stabilizing nanoparticles that are formed, and this eliminates the use of toxic chemicals and external stabilizers (Patra, 2021, Singh, 2023). The application of *Curcuma longa* extract in CuO NPs synthesis has a number of benefits. It offers a renewable and sustainable source of reducing and capping agents that render the synthesis more eco-friendly. Moreover, the extract's bioactive compounds provide functionalities to nanoparticles that enhance their biocompatibility, stability, and potential biological uses. *Curcuma longa*'s inherent anti-inflammatory and antioxidant activities improve the quality of the synthesized CuO NPs and expand their potential in therapeutic applications. In *Curcuma longa*, abundant polyphenols, flavonoids, and curcuminoids act as natural electron donors, reducing Cu^{2+} ions to Cu^{0} nuclei via sequential one-electron transfer steps. These phytochemicals also chelate and cap the nascent particles, preventing uncontrolled growth and agglomeration. Upon subsequent oxidation and calcination, the stabilized nuclei yield uniformly sized CuO nanostructures with controlled sheet-like morphology (VenkatasDaniels and Singh, 2022, Faisal et al., 2021a).

A number of recent reports have demonstrated the green synthesis of CuO

nanoparticles using Curcuma species. For example, (Faisal et al., 2021b) achieved CuO, NiO, and Cu–Ni hybrid nanostructures with antimicrobial and cytotoxic activities, while a comparative study by (Gangal et al., 2025) examined Curcuma amada, C. caesia, C. longa, and C. zedoaria for nanoparticle production. Preliminary reviews of Curcuma longa–derived copper nanoparticles have been provided by (Engku Razali and Othman, 2023), and combined syntheses with Azadirachta indica were investigated by (Murugesan et al., 2023), focusing mainly on antibacterial properties. Although these works confirm the feasibility of Curcuma-mediated routes and report characteristic optical and structural features, they do not systematically vary the metal-precursor concentration or correlate it quantitatively with morphology, crystallinity, and optical response.

To address gaps in prior Curcuma-mediated syntheses, CuO nanostructures were prepared via green synthesis using Curcuma longa extract and systematically varying the copper-acetate precursor concentration from 0.025 to 0.1 M. By combining SEM, XRD, FT-IR, UV–Vis spectroscopy, and EDX, quantitative correlations between precursor concentration and nanoparticle features were established. Notably, an optimal sheet-like morphology with exceptional monodispersity and phase purity was achieved at 0.05 M, offering a scalable, eco-friendly route to CuO nanomaterials. These findings advance the fundamental understanding of plant-mediated growth mechanisms and provide clear guidelines for tuning nanoparticle characteristics for catalysis, sensing, and environmental remediation, highlighting the promise of plant extracts as sustainable alternatives to traditional nanoparticle synthesis.

2. Experimental

2.1. Materials and characterizations

For this work, Sodium hydroxide (NaOH), Copper (II) acetate monohydrate (Cu(CH3COO)2.H2O), and Ethanol (C_2H_6O) were purchased from Merck Company in Germany and used without any treatment. Deionized (DI) water or distilled water was acquired using a high-pure system (Smart-2-Pure).

X-ray diffraction (XRD) patterns were obtained via a PANalytical X'Pert PRO (Cu Kα = 1.5406 Å) with a scanning speed of 1° per minute over a 2θ in the range (20° to 80°). The morphology and size distribution of the particles were examined via scanning electron microscopy (SEM - Quanta 450). The chemical composition of the samples was determined through Energy Dispersive X-ray Spectroscopy (EDX- Bruker Nano Berlin, Germany), conducted within the SEM apparatus. Fourier Transform Infrared (FT-IR) analyse was performed with a Shimadzu ATR-FTIR spectrophotometer featuring a single bounce diamond ATR and a resolution of 4 cm^{-1}. UV-visible spectroscopy analyses were carried out using a Cecil Aquarius CE 9500 Double Beam UV/Visible Spectrophotometers within the 190-1100 nm wavelength range.

2.2. Preparation of Ethanolic Extract of Curcuma longa

The *Curcuma longa* tubers, sourced from Chabahar City, Iran, were thoroughly cleaned to remove soil particles and other impurities. Then the tubers let them to dry under standard sunlight for one week to eliminate moisture. After drying, the tubers were ground to be a fine powder, which was sieved and kept for subsequent use.

The extraction process was carried out by mixing 10 g of *Curcuma longa* powder with 100 ml of ethanol in a flask (200 ml). A magnetic stirrer was used to stir the mixture for 4 hours at 70°C on a hot plate. After stirring, the solution was filtered through a 20 mm filter paper (Whatman) to obtain the ethanolic extract. The role of this extract in the synthesis of CuO NPs is as a reducing and capping agent.

2.3. Green synthesis of CuO NPs

To synthesize CuO NPs, a solution of copper acetate dihydrate was prepared in varying concentrations (S1:0.025 M, S2:0.05 M, S3:0.075 M, and S4:0.1 M) to investigate the effect of precursor concentration. A 100 mL solution of the desired concentration was mixed with 50 mL of *Curcuma longa* extract and then put in a 200 mL beaker. The mixture was stirred at 60 °C for 30 minutes.

Subsequently, 10 drops of NaOH (0.1 M)

were added to fix or adjust the pH value of the mixture, and the stirring was continued for an additional 30 minutes. During this process, the mixture's color changed from yellow to brick brown, which indicates the CuO NPs formation in the solution (Figure 1). To collect the produced nanoparticles, the solution was centrifuged and cleaned by washing and rinsing with distilled water and ethanol to eliminate unreacted materials or impurities. Finally, the purified nanoparticles were calcined at 400 °C in a furnace for 1 hour in the lab atmosphere to enhance their crystallinity.

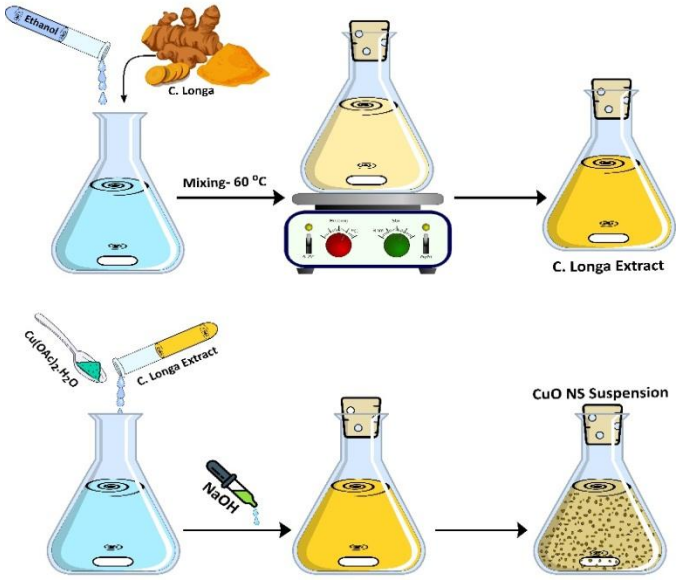

Fig. 1: The process of green synthesis of CuO NPs using *Curcuma longa* extract

3. Results and discussion

3.1. SEM analysis

Figure 2 shows the SEM images of sample 1 (S1), synthesized with a concentration of 0.025 M, the CuO nanostructures exhibit a sheet-like morphology with well-defined and uniform features. These sheet-like structures have an approximate thickness of 20 nm, highlighting their nanoscale dimensions. The nanostructures display low levels of agglomeration, suggesting that the synthesis process, aided by the *Curcuma longa* extract as a capping agent, effectively prevented particle clustering. Additionally, the particles show good size distribution, indicating uniform growth and consistent synthesis conditions. The structures are predominantly monodisperse, with a narrow size distribution, which is desirable for some applications, such as catalysis, sensing, and drug delivery.

The SEM images of sample 2, synthesized with a concentration of 0.05 M, reveal well-defined CuO nanostructures exhibiting a sheet-like morphology (Figure 3). The sheets have an approximate thickness of 18 nm, slightly thinner than those observed in sample 1. The images at different magnifications show low agglomeration, suitable particle size distribution, and a predominantly monodisperse nature.

Compared to sample 1, sample 2 demonstrates improved monodispersity and reduced agglomeration, suggesting that increased precursor concentration to 0.05 M contributes to better nanoparticle dispersion and structural uniformity. These characteristics enhance the quality of the synthesized CuO nanostructures s, making them more suitable for applications requiring highly uniform nanomaterials.

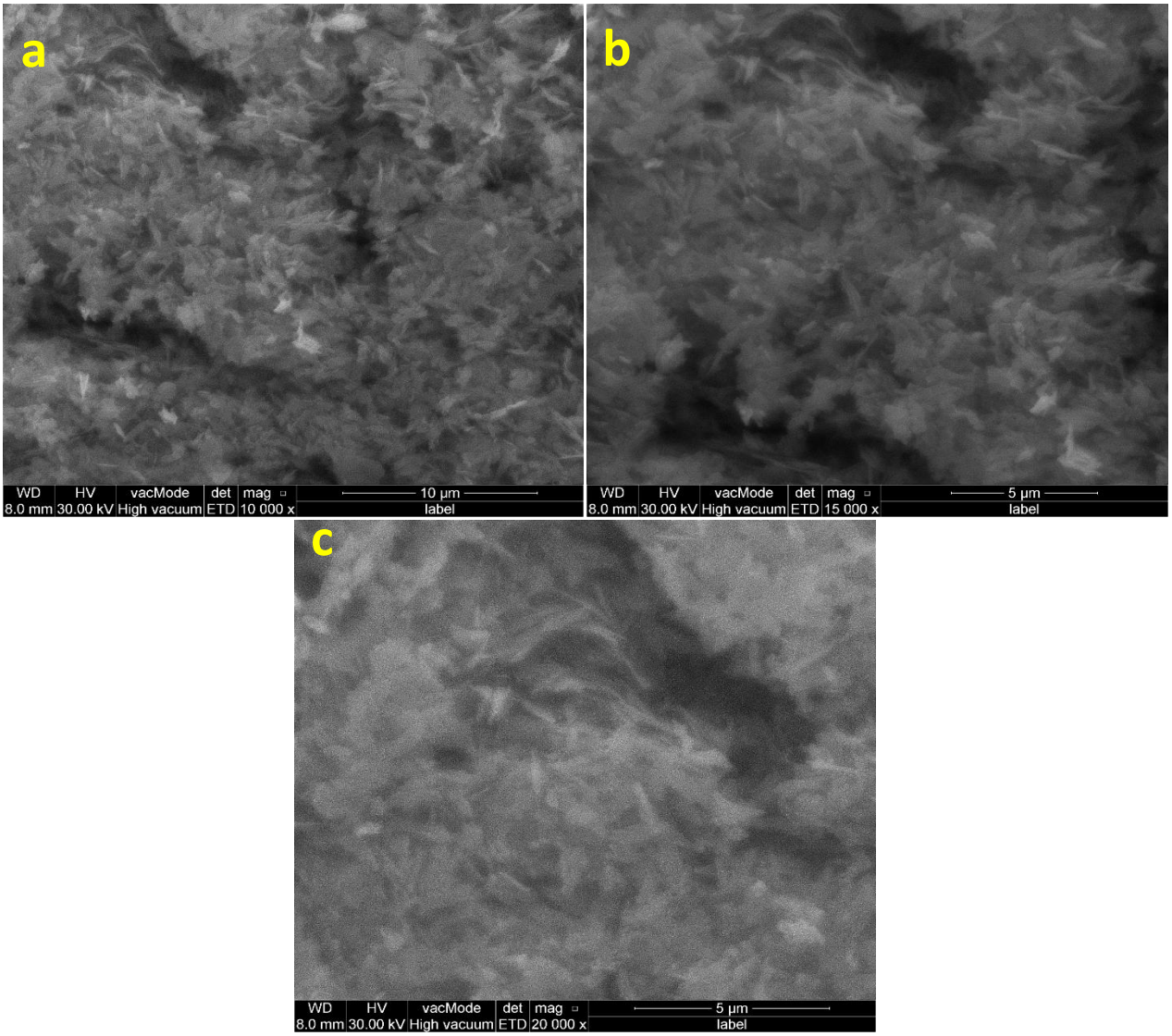

Fig. 2: SEM image of CuO nanostructures synthesized at 0.025 M precursor concentration (S1) showing sheet-like morphology with an average thickness of ~20 nm and minimal agglomeration.

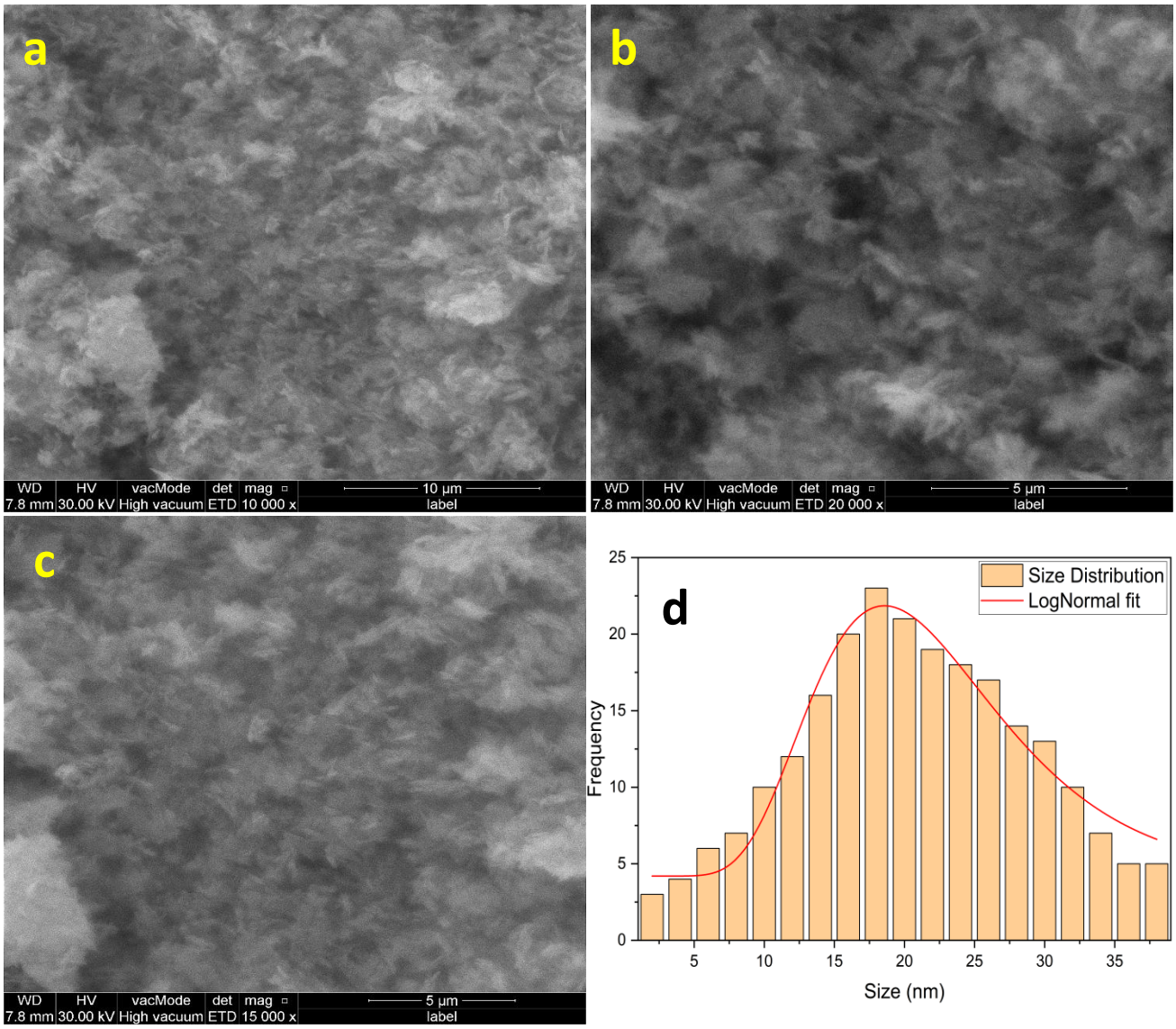

Fig. 3: SEM image and size distribution analysis of CuO NPs synthesized at 0.05 M precursor concentration (S2) showing sheet-like morphology with an average thickness of ~18 nm and minimal agglomeration.

Size distribution analysis (Figure 3d) demonstrates that the CuO nanoparticles exhibit a log-normal distribution with a prominent peak at 15-20 nm, representing the most abundant particle population.

Figure 4 shows the SEM analysis of the CuO nanostructures synthesised with a precursor concentration of 0.075 M (sample 3), the images reveal a considerable change in the size morphology of the CuO nanostructures. Unlike the sheet-like morphology observed in samples 1 and 2, the nanostructures have transitioned to a rod-like morphology with an approximate diameter of 80 nm. The images, taken at different magnifications, show a notable increase in agglomeration as the precursor concentration increases.The particle size distribution has become broader, and monodispersity has decreased, indicating less uniform growth of the nanostructures. The increased agglomeration and particle size suggest that higher precursor concentrations promote rapid nucleation and uncontrolled growth, leading to structural clustering and non-uniformity. Compared to samples 1 and 2, sample 3 demonstrates larger particles, higher agglomeration, and a shift from sheet-like to rod-like morphology, which reflects the effectiveness of precursor concentration on the synthesis process and resulting nanoparticle properties.

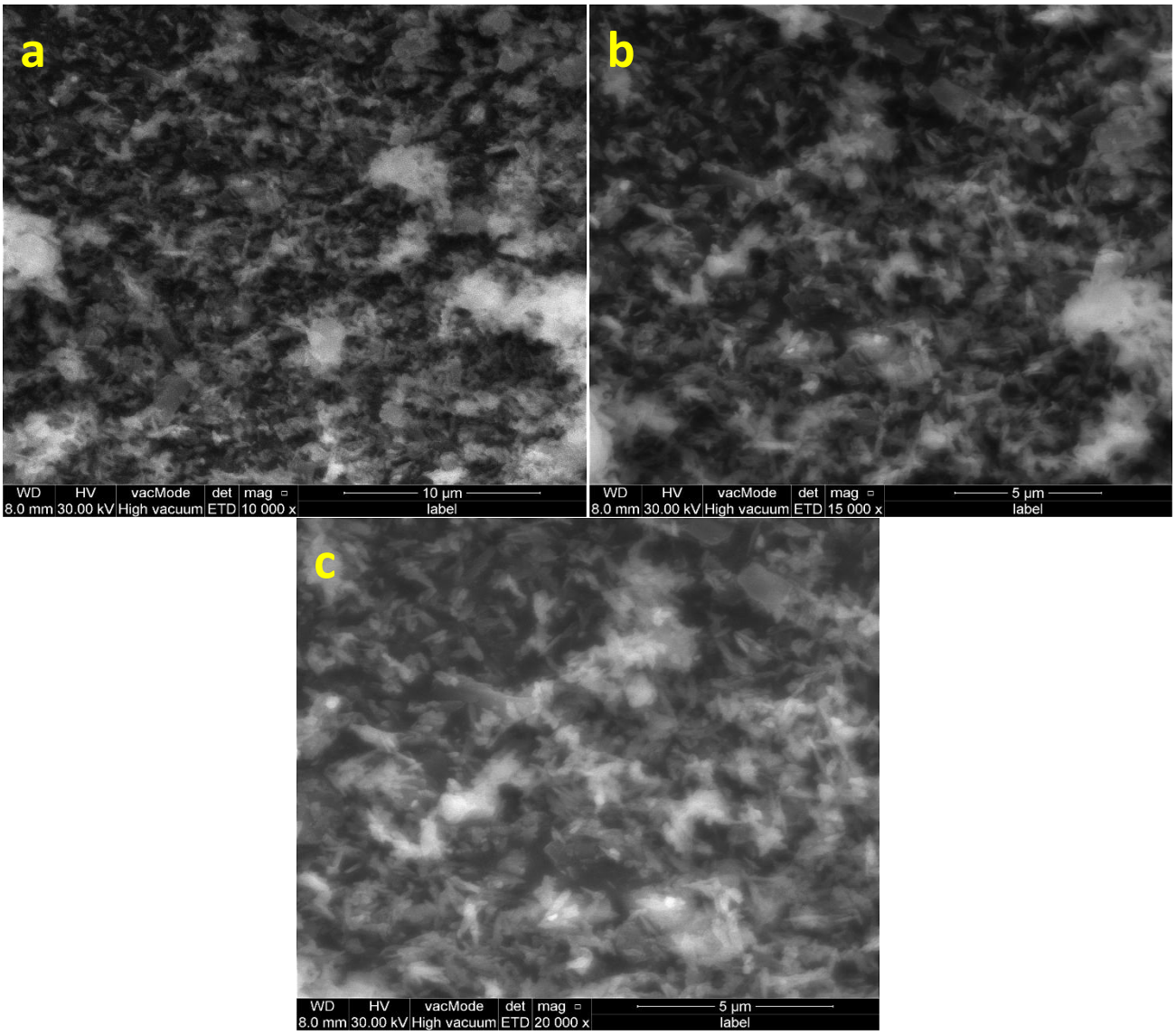

Fig. 4: SEM image of CuO nanostructures synthesized at 0.075 M precursor concentration (S3) showing a transition to rod-like morphology with an average diameter of **~80 nm**.

Figure 5 shows the SEM images of the CuO nanostructures synthesized with a precursor concentration of 0.1 M, which reveals a further morphological transformation of the CuO nanostructures (sample 4 (S4)). In contrast to the sheet-like (S1 and S2) and rod-like morphologies (S3), the nanostructures exhibit a spherical morphology in this sample. The spherical structures have an approximate diameter of 90 nm, which indicates a continued increase in particle size with increasing precursor concentration. The images, captured at different magnifications, show significant agglomeration, progressively increasing as the precursor concentration rises.

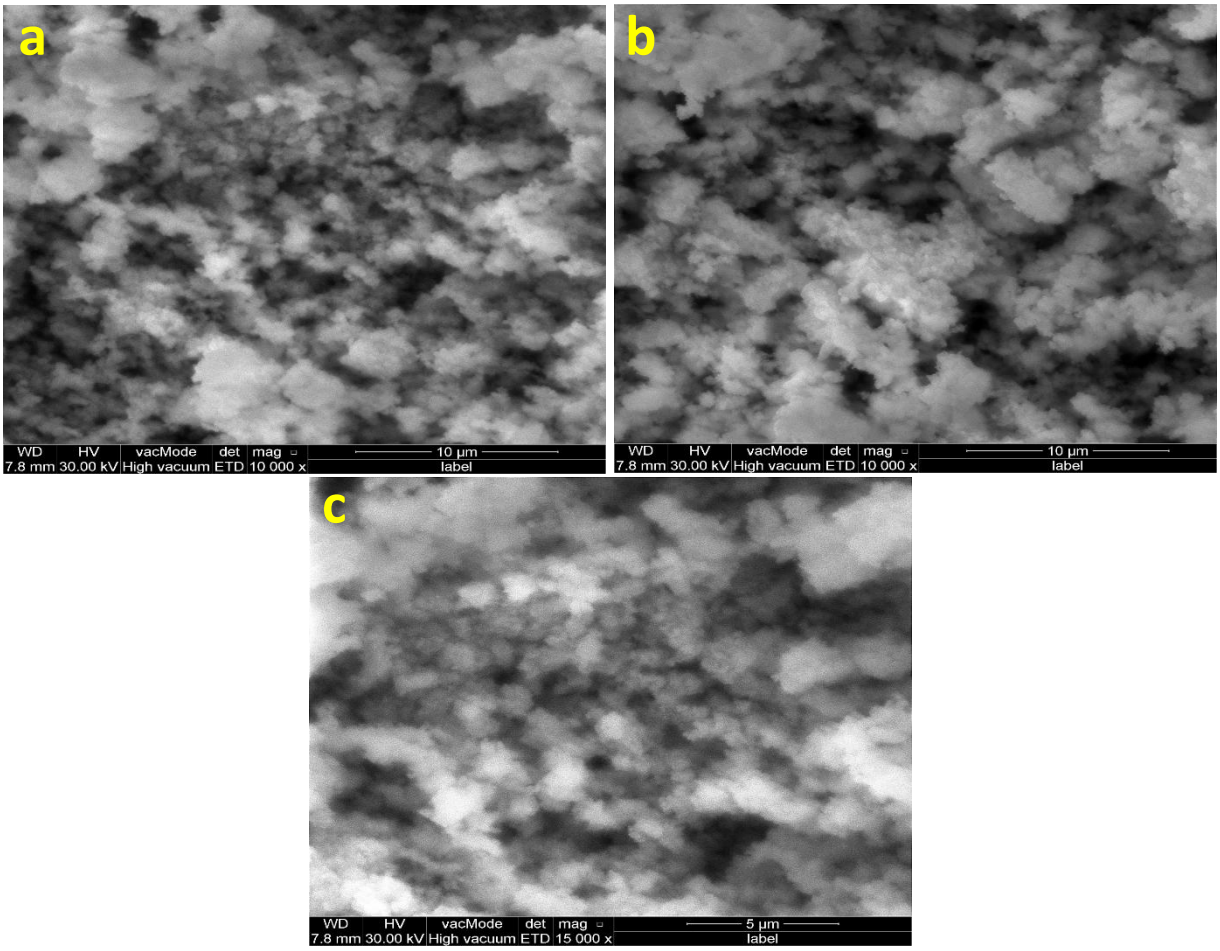

Fig. 5: SEM image of CuO nanostructures synthesized at 0.1 M precursor concentration (S4) showing spherical morphology with an average diameter of **~90 nm**.

Furthermore, the particle size distribution has broadened, and monodispersity has decreased, indicating less uniform growth and a lack of structural control at higher precursor concentrations. Compared to the previous samples, sample 4 demonstrates a shift to spherical morphology, increased agglomeration, and larger particle size, highlighting the substantial impact of the concentration of the precursor on the growth mechanism and morphology of the synthesized CuO nanoparticles.

The SEM analysis revealed a clear trend in the morphology of CuO nanostructures as the precursor concentration was increased from 0.025 M (S1) to 0.1 M (S4). As shown in **Table 1**, at 0.025 M (S1), CuO nanostructures exhibited a sheet-like morphology with an average size of approximately 20 nm and minimal aggregation, indicating a uniform particle size distribution. At 0.05 M (S2), the morphology remained sheet-like but with a slightly smaller average size of 18 nm and very low aggregation, suggesting better nanoparticle dispersion.

At 0.075 M (S3), a transition was observed from sheet-like to rod-like morphology, with an increase in particle size to approximately 80 nm and higher agglomeration. The increased precursor concentration led to broader particle size distribution and decreased uniformity. Finally, at 0.1 M (S4), the morphology shifted to spherical particles, with larger diameters (~90 nm) and very high agglomeration, indicating less control over particle growth.

These SEM observations, summarized in **Table 1**, indicate that a precursor concentration of 0.05 M (S2) resulted in the best-defined, sheet-like CuO nanostructures, with the smallest particle size and minimal agglomeration, making

it the optimal concentration for synthesizing CuO nanoparticles. Further characterizations, including XRD, FT-IR, EDX, and UV-Vis spectroscopy, were performed on sample 2 to evaluate its structural, chemical, and optical properties.

Table 1. SEM Observations Across Different Precursor Concentrations:

Sample	Precursor Conc. (M)	Morphology	Avg. Size	Agglomeration
S1	0.025	Sheet-like	~20	Low
S2	0.05	Sheet-like	~18	Very low
S3	0.075	Rod-like	~80	High
S4	0.1	Spherical	~90	Very high

3.2. FT-IR analysis

The FT-IR spectra of *Curcuma longa* extract and CuO nanostructures (S2) are shown in Figure 6. For the extract, reveals several distinct peaks corresponding to various functional groups, confirming the presence of bioactive compounds responsible for their reducing and capping actions during green synthesis (Figure 6a). The peak position at 3280.99 cm^{-1} is a broad peak that corresponds to O-H stretching vibrations, indicating the presence of hydroxyl groups, likely from phenolic compounds and water molecules. The peak position at 2924.73 cm^{-1} is assigned to C-H stretching vibrations from aliphatic compounds, representing organic molecules in the extract. The peak position at 1624.69 cm^{-1} is a strong peak that corresponds to C=C stretching vibrations, characteristic of aromatic compounds such as curcuminoids and other polyphenols.

The peaks at 1511.21 cm^{-1} and 1430.76 cm^{-1} attributed to aromatic C=C and C-H bending vibrations, further confirming the presence of aromatic functional groups. Peaks corresponding to 1371.87 cm^{-1} and 1277.06 cm^{-1} are attributed to C-O bending and stretching vibrations and are typically characteristic of phenolic or alcoholic groups. Peaks corresponding to 1239.71 cm^{-1} and 1150.64 cm^{-1} corresponding to C-O-C stretching vibrations and indicative of the presence of functional groups. Peak corresponding to 1001.25 cm^{-1} is attributed to C-O stretching vibrations and is presumably due to polysaccharides or other organic compounds in the extract. The peaks of low frequencies at 853.29 cm^{-1}, 811.63 cm^{-1}, and 761.35 cm^{-1} are C-H bending vibrations of aromatic rings and are further evidence of aromatic compounds. Finally, peaks at 570.29 cm^{-1}, 517.14 cm^{-1}, 438.14 cm^{-1}, and 423.77 cm^{-1} can be attributed to vibrations of various organic groups or possible metal-ligand bonding.

The FT-IR spectrum confirms that there are significant bioactive compounds like hydroxyl, carbonyl, and aromatic groups in Curcuma longa extract. These functional groups play an important role as stabilizing and reducing agents while the green synthesis method in the preparation of CuO nanostructures.

The FT-IR spectrum of sample 2 shows the characteristic functional groups and bonds, confirming the successful synthesis of CuO nanostructures (Figure 6b). A peak was observed at 3351.37 cm^{-1}, it is a broad peak that corresponds to the O-H stretching vibrations, indicating the presence of surface hydroxyl groups or adsorbed water molecules. The peak at 1009.87 cm^{-1} attributed to C-O stretching vibrations, likely originating from minor organic residues. Firm peaks at 593.28 cm^{-1} and 497 cm^{-1} are characteristic of Cu-O stretching vibrations, confirming CuO nanostructure formation. These peaks are typical of monoclinic CuO, verifying the structural integrity and

successful synthesis of copper oxide nanoparticles. These bands are in excellent agreement with those reported by Jillani et al. (2018) and Malviya et al. (2015), who observed Cu–O peaks at ~590–600 cm^{-1} and ~490–500 cm^{-1} in plant-mediated CuO NPs, thus verifying the high purity and structural integrity achieved in our green synthesis (Jillani et al., 2018, Malviya et al., 2015).

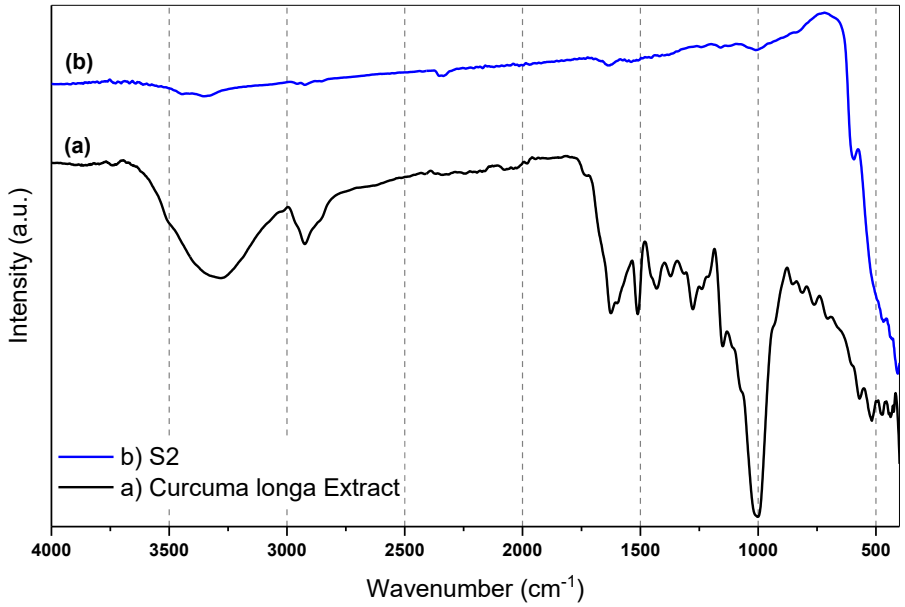

Fig. 6: FT-IR spectrum of (a) *Curcuma longa* extract and (b) CuO nanostructure

Since the sample was calcined at 400 °C, most of the organic components from the *Curcuma longa* extract have decomposed, and their characteristic peaks are no longer visible in the spectrum. The observed peaks primarily correspond to CuO, reflecting the high purity and structural quality of the synthesized nanostructures. Table 2 summarizes the key FTIR peaks observed in the extract and the CuO nanoparticles, providing a clear comparison and highlighting the chemical transformations that occurred during the synthesis process.

Table 2. FTIR Peak Comparison of Curcuma longa Extract and CuO Nanoparticles:

Wavenumber (cm^{-1})	Assignment	Present in Extract	Present in CuO NPs	Interpretation
~3280 / ~3350	O–H stretching (phenols, water)	✓	✓	Surface hydroxyls, bioactive compound residue
~2925	C–H stretching (aliphatic)	✓	X	Lost after calcination
~1625	C=C stretching (aromatic)	✓	X	Degraded upon heating
~1270–1150	C–O / C–O–C (ethers, esters)	✓	X	Removed after calcination
~593 / ~497	Cu–O stretching	X	✓	Confirmation of CuO formation

3.3. UV-visible and Optical Bandgap Analysis of CuO NPs

The UV-Vis spectrum of *Curcuma longa* extract and S2 are shown in Figure 7. For *Curcuma longa* extract it shows two distinct absorption peaks, providing insight into the presence of bioactive compounds within the extract (Figure 7a). The first peak at 240 nm corresponds to π→π* electronic transitions, typically associated with aromatic compounds such as phenolics, flavonoids, or curcuminoids present in the extract. This indicates the presence of conjugated double bonds or aromatic rings, which are common in bioactive molecules.

The second peak at 428 nm is characteristic of n→π* transitions, which are typically attributed to curcuminoids, the main bioactive compounds in *Curcuma longa.* Curcuminoids are strongly absorbed in the visible region due to their extensive conjugation. This peak confirms that there are chromophores in the extract that are accountable for stabilizing and reducing behavior in green synthesis of nanoparticles.

The UV-Vis spectrum of S2 (CuO nanostructure s with concentration of 0.05 M) displays three significant absorption peaks at 207 nm, 310 nm, and 376 nm that are significant to identify optical absorption behavior of synthesized nanostructure (Figure 7b). Absorption peak appearing at 207 nm is attributed to electron transition in organic residues or adsorbed molecules on the surface, presumably residues of Curcuma longa extract used for green synthesis. This peak can be attributed to π→π electronic transition in trace organic compounds. Absorption peak appearing at 310 nm can be attributed to intermediate oxidation states of copper (Cu^{+}/Cu^{2+}), and this can be characteristic of ligand-to-metal charge transfer (LMCT) transition characteristic for CuO nanostructure s synthesized through the green method (Al-Fa'ouri et al., 2023).

The highest absorption peak position of 376 nm is characteristic for monoclinic CuO and is due to valence to conduction band charge transfer. This peak is in accordance with literature reported values for CuO nanostructures (Prasad, 2019). Further, broad absorption greater than 400 nm in the visible region is in accordance with CuO having a semiconducting nature and having a narrow bandgap and is best suited for use in photocatalysis and optoelectronics.

Overall, the UV-Vis absorption spectrum confirms the successful formation of CuO nanostructures with well-defined optical properties and structural integrity. This absorption peak at 376 nm aligns closely with values reported in plant-mediated CuO nanoparticle syntheses, which typically fall in the 375–380 nm range (Prasad, 2019, Al-Fa'ouri et al., 2023).

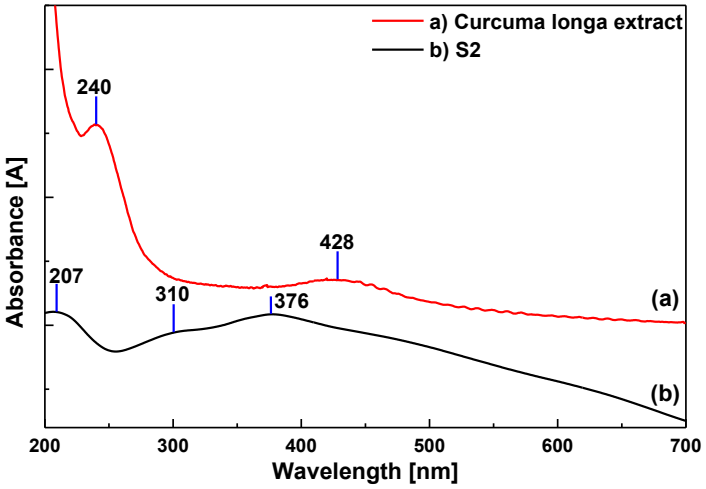

Fig. 7: UV-Vis absorption spectrum of (a) *Curcuma longa* extract and (b) CuO nanostructure

The Tauc plot analysis of the CuO NPs was performed to determine their optical bandgap energy. The optical bandgap of the synthesized CuO NPs was determined using Tauc plot analysis (Figure 8).The plot of $(\alpha h\nu)^{1/2}$ versus photon energy ($h\nu$) exhibited a linear region, characteristic of an indirect bandgap semiconductor. By extrapolating this linear portion to the x-axis, the optical bandgap was estimated to be 1.65 eV, which is consistent with reported values for CuO nanostructures. The slight increase compared to bulk CuO (~1.4 eV) suggests the presence of quantum confinement effects due to the nanoscale dimensions of the particles. The use of $(\alpha h\nu)^{1/2}$ confirms that the electronic transition in these NPs is indirect, involving phonon-assisted processes. This

bandgap value indicates that the CuO NPs are well-suited for visible-light-driven applications, such as photocatalysis, photovoltaics, and gas sensing. The absence of significant sub-bandgap absorption suggests minimal defect-related states, though further analysis (e.g., Urbach energy) could provide deeper insight into the material's disorder.

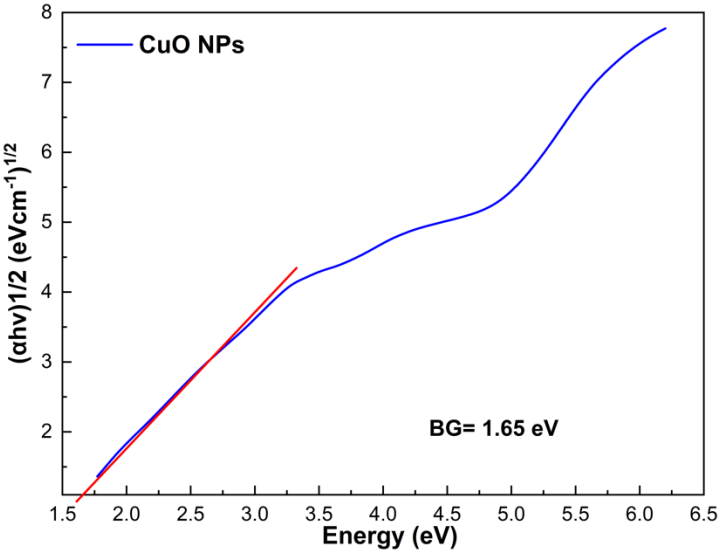

Fig. 8: Tauc plot for CuO nanostructures (S2)

3.4. XRD-EDS analysis

The XRD pattern for S2, shown in Figure 9, reveals a series of distinct diffraction peaks corresponding to the crystalline structure of CuO. The identified peaks at specific 2θ values, including 12.25°, 31.14°, 34.97°, 38.34°, 44.70°, 48.38°, 53.11°, 57.97°, 61.17°, 65.65°, and 74.70°, indexed to the monoclinic phase of CuO, consistent with the standard ICSD reference code for CuO (ICSD 98-006-9758) (Zhang and Xu, 2024). The highest intensity peak, observed at 34.97°, corresponds to the (11-1) plane and represents the most crystalline phase in the sample. This peak is the sharpest, signifying that the corresponding plane has the most dominant crystallite orientation and the highest degree of crystallinity in the sample. The intensity of the peak provides insight into the crystallinity, with sharper and more intense peaks generally indicating better crystalline quality. To estimate the crystallite size, the broadening of the maximum peak was analyzed using the Debye–Scherrer equation:

$$D = \frac{K\lambda}{\beta cos\theta}$$

where D is the crystallite size, K is the Scherrer constant (0.9), λ is the X-ray wavelength (1.5406 Å), β is the full width at half maximum (FWHM) of the peak, and θ is the Bragg angle. Using this equation, the crystallite size was calculated to be **6.6 nm**, which aligns well with the SEM observations of small, uniform nanoparticles. These values closely match those reported by (Zhang and Xu, 2024) and (Prasad, 2019), who documented diffraction peaks near 35° and crystallite sizes of 5–8 nm for green-synthesized CuO nanostructures. This agreement verifies that our Curcuma longa–mediated method yields phase-pure, highly crystalline CuO nanostructures comparable to other eco-friendly approaches.

The XRD analysis validates the formation of highly crystalline and phase-pure CuO nanostructures s. The well-defined peaks confirm the structural quality of the nanostructures, supporting the results obtained from SEM, FT-IR, and UV-Vis analyses. This demonstrates that the green synthesis method using Curcuma longa extract at 0.05 M precursor concentration successfully produced CuO nanostructures.

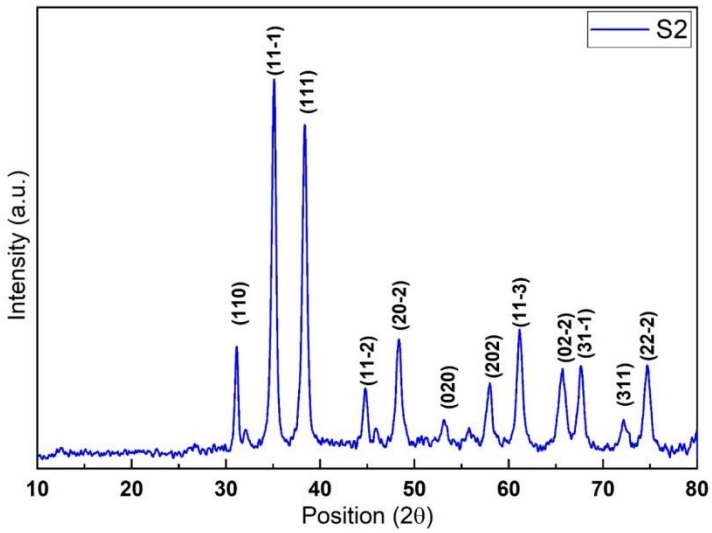

Fig. 9: XRD pattern of CuO nanostructures synthesized at 0.05 M precursor concentration (S2). The diffraction peaks are indexed to the monoclinic phase of CuO, with the highest intensity peak corresponding to the (11-1) plane at 34.97°.

The EDX analysis for sample S2 provides both the elemental spectrum and quantitative results (Figure 10a), along with the elemental mapping image (Figure 10b), confirming the composition and distribution of the synthesized CuO nanostructures. The EDX spectrum confirms the existence of Cu and O as the primary elements, with no detectable impurities. The two strong peaks at approximately 1 keV and 8 keV correspond to the characteristic Cu-Kα and Cu-Lα emissions, indicating the presence of the Cu element. The peak around 0.5 keV corresponds to the O-Kα emission, showing the presence of the O element. Additionally, small peaks near 3 keV are observed, which are attributed to silver used for coating the sample. This silver coating was applied to prevent overcharging during the electron microscopy analysis and improve conductivity, which is a standard procedure in SEM and EDS analyses.

In Figure 10b, the elemental mapping image shows a uniform distribution of both copper and oxygen across the nanostructures s. The consistent spatial overlap of Cu and O signals further supports the successful preparation of CuO nanostructures and the homogeneity of the sample. The elemental composition validates the successful formation of CuO nanostructures with high purity, further supporting the efficiency of the green synthesis method using Curcuma longa extract.

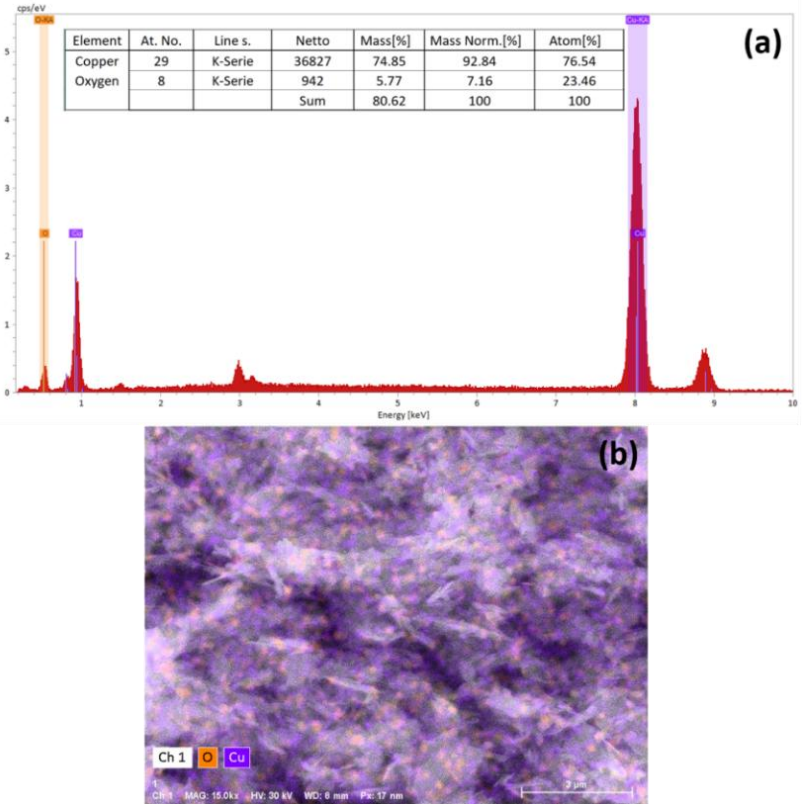

Fig. 10: EDS spectra and elemental analysis of S2 (CuO nanostructures, 0.05)

4. Conclusions

In this study, CuO NPs were successfully prepared via a green synthesis approach with *Curcuma longa* extract as a reducing and capping agent. By varying the precursor concentration, the effect on morphology, size of the nanoparticles, and dispersion of the nanostructures was systematically investigated. SEM results revealed that sample 2, synthesized at 0.05 M precursor concentration, exhibited the best characteristics, including a well-defined sheet-like morphology, improved monodispersity, minimal agglomeration, and smaller particle size with an approximate sheet thickness of 18 nm. FTIR analysis validated the presence of Cu-O bonds, confirming the formation of CuO nanostructures with high purity after calcination at 400°C. The UV-Vis spectrum showed a characteristic absorption peak at 376

nm, highlighting the semiconducting nature of the nanostructures s. XRD analysis demonstrated a highly crystalline monoclinic phase with sharp diffraction peaks and no impurities, while EDX confirmed the elemental composition and uniform distribution of copper and oxygen.

Overall, it can be concluded that the green synthesis process using *Curcuma longa* extract is an effective, eco-friendly, and sustainable method for producing CuO NPs. The optimized precursor concentration of 0.05 M resulted in nanoparticles with superior morphology, crystallinity, and purity, making them suitable for various applications, such as catalysis, sensing, and environmental remediation.

Acknowledgment

The author wishes to express his sincere gratitude to the Scientific Research Center (SRC) of Soran University for their valuable support in the characterization tests that significantly enhanced this research. Their expertise and technical assistance were crucial in the completion of this work. I deeply appreciate their contributions and dedication to advancing scientific knowledge.

Funding

* The author did not receive support from any organization for the submitted work.

Conflicts of interest

The author of this manuscript has no conflicts of interest to disclose. I affirm that there are no financial, personal, or professional relationships that could potentially influence or bias the content of my work.

References

AL-FA'OURI, A. M., ABU-KHARMA, M. H., AWWAD, A. M. & ABUGAZLEH, M. K. 2023. Investigation of optical and structural properties of copper oxide nanoparticles synthesized via green method using Bougainvillea leaves extract. *Nano-Structures & Nano-Objects,* 36**,** 101051.

ALHAMDI, H. W., MAJANI, S. S., DILLIRAJ, S., SEAL, A., NAGESH, N., SHIVAMALLU, C. & KOLLUR, S. P. 2024. Exploring the anticancer potency and photocatalytic efficiency of bio-derived CuO nanoparticles using Moringa oleifera leaf extract. *Results in Chemistry,* 7**,** 101430.

BHUVANESHWARI, V., VAIDEHI, D. AND LOGPRIYA, S., 2018. Green synthesis of copper oxide nanoparticles for biological applications. *Microbiol Curr Res,* 2**,** 9-10.

ENGKU RAZALI, E. N. Z. & OTHMAN, S. A. 2023. Characterization of Synthesized Copper Nanoparticles from Curcuma Longa: A Preliminary Review. *Journal of Research in Nanoscience and Nanotechnology,* 9**,** 42-53.

FAISAL, S., AL-RADADI, N. S., JAN, H., ABDULLAH, SHAH, S. A., SHAH, S., RIZWAN, M., AFSHEEN, Z., HUSSAIN, Z. & UDDIN, M. N. 2021a. Curcuma longa mediated synthesis of copper oxide, nickel oxide and Cu-Ni bimetallic hybrid nanoparticles: characterization and evaluation for antimicrobial, anti-parasitic and cytotoxic potentials. *Coatings,* 11**,** 849.

FAISAL, S., AL-RADADI, N. S., JAN, H., ABDULLAH, SHAH, S. A., SHAH, S., RIZWAN, M., AFSHEEN, Z., HUSSAIN, Z., UDDIN, M. N., IDREES, M. & BIBI, N. 2021. Curcuma longa Mediated Synthesis of Copper Oxide, Nickel Oxide and Cu-Ni Bimetallic Hybrid Nanoparticles: Characterization and Evaluation for Antimicrobial, Anti-Parasitic and Cytotoxic Potentials. *Coatings* , 11, 849.

FUKU, X., THOVHOGI, N. AND MAAZA, M., . Photocatalytic effect of green synthesised CuO nanoparticles on selected environmental pollutants and pathogens. . AIP conference proceedings 2018. AIP Publishing.

GANGAL, A., K., S. N., MANISHA, D., K., S. R., DHEERAJ, B., SINGH, R. V., H., L., SHAVKATZON, A. & AND KUMAR, D. 2025. Green nanotechnology: nanoparticle synthesis using Curcuma amada, Curcuma caesia, Curcuma longa, and Curcuma zedoaria. *Green Chemistry Letters and Reviews,* 18**,** 2449122.

GOTA, T., PRAGYA KULKARNI 2024. Bacterial mediated synthesis and characterization of copper oxide nanoparticles and their antimicrobial and dye remediation applications. *Spectrum of Emerging Sciences,* 11, 4.

GRIGORE, M. E., BISCU, E.R., HOLBAN, A.M., GESTAL, M.C. AND GRUMEZESCU, A.M., 2016. Methods of synthesis, properties and biomedical applications of CuO nanoparticles. *Pharmaceuticals,* 9**,** 75.

JAYARAMBABU, N., AKSHAYKRANTH, A., RAO, T.V., RAO, K.V. AND KUMAR, R.R., 2020. Green synthesis of Cu nanoparticles using Curcuma longa extract and their application in antimicrobial activity. *Materials Letters,* 259, 126813.

JAYASIMHA, H. N., CHANDRAPPA, K.G., SANAULLA, P.F. AND DILEEPKUMAR, V.G., 2024. Green synthesis of CuO nanoparticles: A promising material for photocatalysis and electrochemical sensor. *Sensors International,* 5, 100254.

JEEVANANDAM, J., KIEW, S.F., BOAKYE-ANSAH, S., LAU, S.Y., BARHOUM, A., DANQUAH, M.K. AND RODRIGUES, J., 2022. Green approaches for the synthesis of metal and metal oxide nanoparticles using microbial and plant extracts. *Nanoscale,* 14**,** 2534-2571.

JILLANI, S., JELANI, M., HASSAN, N. U., AHMAD, S. & HAFEEZ, M. 2018. Synthesis, characterization and biological studies of copper oxide nanostructures. *Materials Research Express,* 5**,** 045006.

MALVIYA, N., CARPENTER, G., OSWAL, N. & GUPTA, N. 2015. Synthesis and characterization of CuO nano particles using precipitation method. *AIP Conference Proceedings,* 1665, 050038.

MATHANMOHUN, M., SAGADEVAN, S., RAHMAN, M.Z., LETT, J.A., FATIMAH, I., MOHARANA, S., GARG, S. AND AL-ANBER, M.A., 2024. Unveiling sustainable, greener synthesis strategies and multifaceted applications of copper oxide nanoparticles. *Journal of Molecular Structure,* 1305, 137788.

MISHRA, S. R. A. A., M., 2022. CuO and CuO-based nanocomposites: Synthesis and applications in environment and energy. *Sustainable Materials and Technologies,* 33, e00463.

MURUGESAN, S., MUTHAIAH, D., MUTHUSAMY, Y., GANESAN, S. & MOHAMED MYDEEN, A. K. 2023. Green synthesis of Copper Nanoparticles using Curcuma longa (L.) and Azadirachta indica (L.) and their Antibacterial Activity. *Journal of Medicinal plants and By-Products,* 12**,** 449-458.

OKOYE, P. C., AZI, S. O., QAHTAN, T. F., OWOLABI, T. O. & SALEH, T. A. 2023. Synthesis, properties, and applications of doped and undoped CuO and Cu2O nanomaterials. . *Materials Today Chemistry,* 30**,** 101513.

PATRA, D. A. E. K., R., 2021. Curcumin as a novel reducing and stabilizing agent for the green synthesis of metallic nanoparticles. *Green Chemistry Letters and Reviews,* 14**,** 474-487.

PRASAD, A. S. 2019. Green synthesis and spectral analysis of surface encapsulated copper (II) oxide nanostructures. *Materials Science-Poland,* 37**,** 503-509.

S NAZ, A. G., M ZIA, R JAVED 2023. Synthesis, biomedical applications, and toxicity of CuO nanoparticles *Applied Microbiology and Biotechnology* 107**,** 1039-1061.

SHUKLA, H. 2022. Antibacterial and morphological studies of plant-mediated synthesized CuO nanoparticles using Azadirachta indica (neem) leaf extract. *International Journal of Nano Dimension,* 13, 197-204.

SINGH, H., DESIMONE, M.F., PANDYA, S., JASANI, S., GEORGE, N., ADNAN, M., ALDARHAMI, A., BAZAID, A.S. AND ALDERHAMI, S.A., 2023. Revisiting the green synthesis of nanoparticles: uncovering influences of plant extracts as reducing agents for enhanced synthesis efficiency and its biomedical applications. *International journal of nanomedicine,* 18**,** 4727-4750.

VENKATAS, J., DANIELS, A. & SINGH, M. 2022. The potential of curcumin-capped nanoparticle synthesis in cancer therapy: a green synthesis approach. *Nanomaterials,* 12**,** 3201.

ZHANG, J. & XU, J. 2024. Fabrication of porous copper oxide nanostructure on nickel foam electrode by a co-precipitation method for non-enzymatic glucose detection. *Microchemical Journal,* 203**,** 110864.

ZHIAN, H., KHOJASTEH, H., NIKMARAM, S. & AZIMI, C. 2024. Eco-friendly hydrothermal synthesis of CuO nanoparticles using natural materials as reducing and capping agents. *Iranian Journal of Chemistry and Chemical Engineering,* 43**,** 946-955.